physica status solidi b

phys. stat. sol. (b) **243**, No. 6, 1276–1285 (2006) / **DOI** 10.1002/pssb.200541365

Some electronic and optical properties of self-assembled quantum dots: asymmetries in a lens domain

A. H. Rodríguez* and **L. Meza-Montes**

Instituto de Física, Universidad Autónoma de Puebla, Apdo, Postal J-48, Puebla, Pue. 72570, México

Received 14 October 2005, revised 20 January 2006, accepted 10 February 2006
Published online 21 March 2006

PACS 73.21.La, 73.22.Dj, 78.67.Hc

The self-assembled quantum dot with lens domain has rotational symmetry but it is intrinsically asymmetric when the electron moves perpendicularly to its circular base, i.e. along the rotational axis. To characterize this asymmetry, an external electric field is applied along either the positive or negative direction of the rotational axis. We report the different Stark shifts appearing in the spectra as a function of the field intensity for different lens domains. It is shown that for a flat lens domain the asymmetry effects decrease, but even for very flat lenses they can not be approximated by a cylindrical domain. Finally, some optical properties such as the dielectric constant and electroabsorption are studied. Signatures of the energy spectrum reveal in these quantities. The importance of considering the proper lens domain as long as the magnitude and direction field to tune a specific level transition is stressed.

1 Introduction

Quantum dot (QD) structures have attracted the interest of theoretical and experimental research due to the novel properties they exhibit as a consequence of spatial confinement [1, 2]. The modern growth techniques have led to the self-assembled quantum dot [3]. The experimental and theoretical work related to the optical and electrical study of the properties of quantum dots modelled as pyramids is intense [4–8]. They have also been modelled as quantum disks [9, 10] and spherical quantum dots [11–13]. Nevertheless, under certain growing conditions, these quantum dots have proven to have lens shape geometry characterized by a spherical cap [14–19]. The electronic properties of this so-called self-assembled quantum lens (SAQL) have been studied previously [20, 21]. The study has also included the effects of external electric field [22–25]. Some optical properties of such structures have been analyzed [26].

Recently, it has been characterized the vertically self-organized growth of InAs quantum dots separated by GaAs layers [27]. In Refs. [28] and [29] an effective-mass envelope-function theory has been applied to study the electron and hole energy levels, the wave function, the optical transition matrix elements, excitonic states and optical-absorption spectra of these strained InAs/GaAs quantum dots. In this case, the dots have been modelled by a cylindrical domain of height h and radius R.

The lens domain is limited by the interception of two boundaries, one given by the surface of a spherical cap with certain curvature, and the other a flat boundary. This yields an asymmetric behaviour of the charge carriers as they are pushed toward either surface. Consequences of this spatial asymmetry were

* Corresponding author: e-mail: arezky2000@yahoo.com
Present address: Instituto de Física, Universidad Nacional Autónoma de México (UNAM), Apdo. Postal 20-364, San Angel 01000, México DF., México

first reported in Ref. [30] for microphotoluminescence measurements and were qualitatively reproduced in Ref. [31].

In case of a very flat lens domain, the two boundaries will be almost equal and the domain could be similar to a cylindrical domain. Nevertheless, here we will show that the cylindrical domain can not be used to reproduce the electrical and optical properties of a flat lens domain.

The present work is devoted to study in more details the asymmetry effects on the electronic and optical properties of different lens configurations. It will be shown that in the presence of an external electric field, the electronic and optical properties have different behaviour depending on whether the field is along the positive or negative direction of the axial axis.

2 Electronic structure

We will consider a typical SAQL that presents a circular cross section of radius a and maximum cap height b with $b < a$. The lens base lies on the xy-plane and the axial symmetric axis is along the z-axis. We want to explore the implications of the different shapes of the lens boundaries on the physical parameters of the SAQL, such as energy levels and wavefunctions. Thus, the SAQL will be under an external electric field F which will be along either the positive or negative direction of the z-axis.

The exciton wave functions are solutions of

$$\left[-\frac{\hbar^2}{2m_{\mathrm{e}}^*}\nabla_{\mathrm{e}}^2-\frac{\hbar^2}{2m_{\mathrm{h}}^*}\nabla_{\mathrm{h}}^2-e\boldsymbol{F}(\boldsymbol{r}_{\mathrm{e}}-\boldsymbol{r}_{\mathrm{h}})-\frac{e^2}{\varepsilon|\boldsymbol{r}_{\mathrm{e}}-\boldsymbol{r}_{\mathrm{h}}|}\right]\Psi_{N_{\mathrm{e}},N_{\mathrm{h}}}(\boldsymbol{r}_{\mathrm{e}},\boldsymbol{r}_{\mathrm{h}})=(E-E_{\mathrm{g}})\,\Psi_{N_{\mathrm{e}},N_{\mathrm{h}}}(\boldsymbol{r}_{\mathrm{e}},\boldsymbol{r}_{\mathrm{h}})\,, \tag{1}$$

where E_{g} is the gap energy, ε is the dielectric constant, and m_i^* is the quasiparticle effective mass with $i = \{\mathrm{e}, \mathrm{h}\}$, e (h) denoting electron (hole).

Closed solutions of one-particle wave functions $\Psi_{N,m}$ and energy levels $E_{N,m}$ as a function of the applied electric field and lens geometry have been published elsewhere [21, 31]. Here, N enumerates, for a fixed value of m, the electronic levels by increasing value of energy, and m is the z component of the orbital angular momentum. The excitonic correction appearing in Eq. (1) has been considered in first order perturbation theory. Details can be seen in Ref. [26].

2.1 Asymmetry of the ground state transition energy

In order to explore the effect of spatial asymmetry on the lens spectra, we have defined for a given material the parameter

$$\delta(F) = E_{\mathrm{T}}(+F) - E_{\mathrm{T}}(-F)\,, \tag{2}$$

where E_{T} is the ground state transition energy. For an electric field of magnitude F the parameter $\delta(F)$ measures the difference between the transition energies for the fields along the positive direction $+F$ and the negative direction $-F$.

In Fig. 1(a) we show the parameter $\delta(F)$ as a function of b/a for two values of the electric field and dots different materials, InAs/GaAs and CdSe/ZnSe. The unit of energy is $E_0 = \hbar^2/2m_{\mathrm{e}}V_0^{2/3}$, where m_{e} is the free electron mass and the unit of electric field is $F_0 = E_0/eV_0^{1/3}$. We have used $m_{\mathrm{e}}^*/m_{\mathrm{e}} = 0.023$ and $m_{\mathrm{hh}}^*/m_{\mathrm{e}} = 0.34$ for InAs [9] whereas $m_{\mathrm{e}}^*/m_{\mathrm{e}} = 0.11$ and $m_{\mathrm{hh}}^*/m_{\mathrm{e}} = 0.44$ for CdSe [32].

The parameter V_0 is the volume of the lens domain. It is related to the deformation b/a and the radius a of the domain through the expression:

$$V_0 = \frac{1}{2}\pi a^3\left(\frac{b}{a}\right)\left[1+\frac{1}{3}\left(\frac{b}{a}\right)^2\right]. \tag{3}$$

Thus, the lens domain can be defined by three parameters: the volume V_0, the radius a and the deformation b/a, but only two of them are independent. The confinement regime is determined by the volume

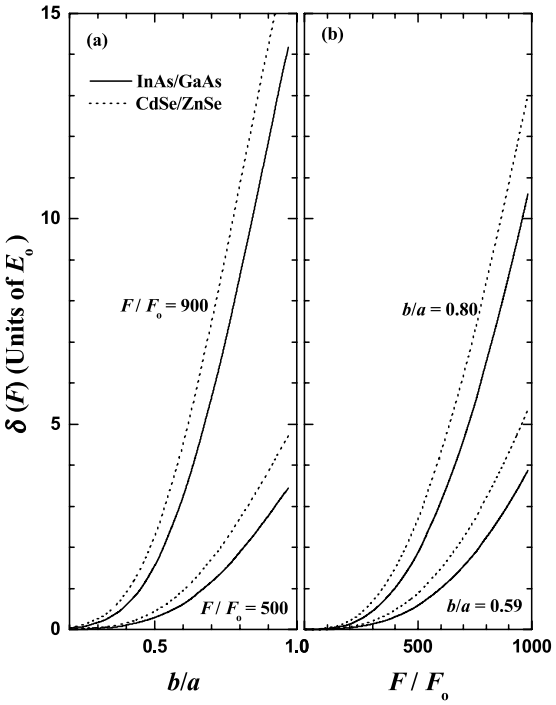

Fig. 1 Parameter δ as a function of (a) the lens domain deformation b/a for two values of the electric field, and (b) the absolute value of the electric field F for two lens configurations. For solid line the InAs parameters were used whereas the dotted line refers to CdSe SAQDS.

V_0 of the domain and the deformation b/a. If one of them decreases, the energy levels increase. We want to study the effects on the energy levels by changes of the lens domain but not in terms of the confinement caused by the volume variation. Therefore, in Fig. 1(a) the lens volume is kept fixed as b/a is modified.

In Fig. 1(b) the values of δ are shown, now as a function of the absolute value of the electric field for two different lens domains given by the indicated values of b/a. Similarly to Fig. 1(a), the volume V_0 has been fixed.

It can be seen in both figure that as b/a decreases, so does the value of δ. This could be expected due to the fact that, as the lens domain becomes flatter, the two boundaries turn out to be more similar and then the asymmetry along the axial axis "is reduced". Thus, higher field intensities F are necessary to increase the value of δ for small b/a ratio. Notice also that for the CdSe SAQL, the values of δ are higher compared to those of the InAs dot. This effect is produced by the effective mass which in the CdSe material is higher for both the electron and heavy hole. Then the energy of the ground state transition is lower than the InAs case, and the contribution of the electric field to the energy is higher that in the InAs case for a given value of F.

Higher states are less affected by the field because its energy contribution is then relatively lower [24]. Lower values of δ would be expected for both materials in these cases. Therefore, for a flat enough lens domain ($b/a \ll 1$) and not too high values of the electric field, the asymmetry in the values of the ground and the first excited states transition energies could be neglected. This could suggest to employ simpler geometries, as we now discuss.

2.2 Comparison between lens and cylindrical domains

Due to the results obtained in the previous section, one could ask if a strongly deformed lens ($b/a \ll 1$) could be approximated by a cylindrical domain with radius R, height h and the same volume V_0. The cylinder parameters should be selected in such a way that the cylinder shape resembles the lens domain.

We have now the problem of selecting properly the values of R and h to obtain energy levels the more similar to those of the lens. It is also necessary to take into account that the energy levels in the cylindrical domain are given by

$$E_{n,l,k}^{(\mathrm{cil})} = \frac{\hbar^2}{2m^*}\left(\frac{\mu_{n,l}^2}{R^2} + \frac{k^2\pi^2}{h^2}\right), \tag{4}$$

where $\mu_{n,l}$ is the n-th zero of the Bessel function J_l with $l = 0, 1, 2, \ldots$ and $k = 1, 2, \ldots$ is the quantum number associated with the quantization of the linear momentum along the axis of the cylindrical domain.

We impose two conditions for any value of b/a: (i) the cylinder and lens domains have the same volume V_0 which is kept constant, and (ii) the ground state of both domain geometries are the same. This allows us to select suitable values of R and h and to find out if the first excited states of the cylinder are rather close to those of the corresponding lens.

There are two possible cylinder configurations which fulfill the former conditions for a given value of b/a. One of them consists of a very high cylinder with $h \gg b$ and small R. This configuration is not considered here, instead we consider the other one since it resembles the lens domain. In Fig. 2(a) we can see the behaviour of R and h as a function of b/a, for a cylinder domain which fulfills the conditions (i) and (ii). The ratio R/a is almost constant and we have $R/a < 1$. Contrary, the ratio h/a strongly decreases with b/a. The dotted line maps directly the values of b/a onto the vertical axis. Comparing this dotted line with h/a we conclude that $h/a < b/a$ for the shown range of b/a. Consequently, we can see that h is also smaller than the lens height b and for $b/a \to 0$ we have that $h \to b$.

In Fig. 2(b) we have plotted using continuous lines the first two energy levels of the lens domain as a function of b/a. We have included also in dotted lines the first six energy levels of the cylindrical configuration using Eq. (4) with the parameters R and h shown in Fig. 2(a). In this case, the energy unit is $E_0 = \hbar^2/2m^*V_0^{2/3}$, with m^* the effective mass. Then, the plot shows the universal behaviour of the energy levels of the lens and cylindrical domain for any material having effective mass m^*. The quantum numbers are shown in the figure.

To analyze Fig. 2 it is important to take into account that as the lens parameter b/a decreases the radius a increases, for a given value of the volume V_0. See Eq. (3). The behaviour of R and h in Fig. 2(a) and Eq. (4) suggest that the cylinder levels of Fig. 2(b) can be approximated for $b/a \ll 1$ by the expression

$$E_{n,l,k}^{(\mathrm{cil})} \approx \frac{\hbar^2}{2m^*}\frac{k^2\pi^2}{h^2}\,. \tag{5}$$

This shows why cylinder levels with the same k tend to cluster in the $b/a \ll 1$ regime though a finite separation remains which depends on the cylinder radius according to Eq. (4). This clustering, driven by the symmetry along the axial axis, does not appear in the lens levels where this symmetry is lacking and is reflected in the fact that only two quantum numbers charaterize the states. See Fig. 2(b).

It can be concluded then that the first excited levels of a flat lens can not be approximated by those of a cylindrical domain with same volume and ground state energy.

3 Lens domain: influence of asymmetry on the optical properties

The asymmetry found in the energy levels for positive and negative electric fields is not the only possible effect of the domain asymmetry along the axial axis. The wavefunctions are also affected by the different curvatures of the boundaries, depending on the direction of the electric field. It also gives rise to asymmetry in other physical properties. See for example Fig. 2 in Ref. [31], where differences in the carrier polarizations and the oscillator strengths were reported. One way to study the combined influence of asymmetry on the shifts of the transition energy and the oscillator strengths is through the dielectric constant.

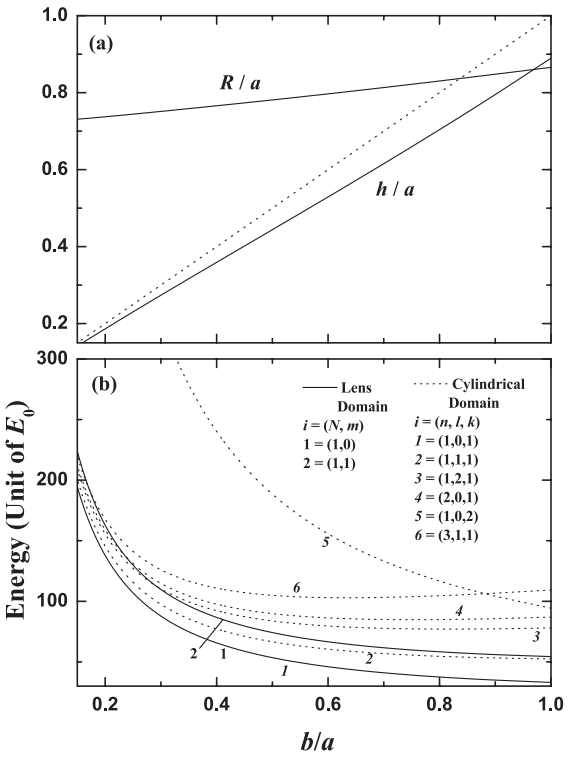

Fig. 2 (a) Behaviour of R and h as a function of b/a for a cylindrical configuration which fulfills conditions (i) and (ii). (b) First two energy levels of the lens domain and first six energy levels of the cylindrical domain as a function of b/a. Level quantum numbers are also shown in the figure. See text.

In the following, we analyze the imaginary part of the dielectric constant for the case of InAs/GaAs SAQLs by comparing two lens configurations. Due to the axial symmetry of the SAQL, the interband selection rules correspond to excitonic branches such that $m_c - m_v = 0$, where $m_c(m_v)$ is the z-projection of the angular momentum in the conduction (valence) band. We have only considered incident frequencies in the range below the band offset, according to the material parameters listed in Table 3, where m^* is the effective mass of the particle in the conduction c or valence bands hh and lh, P is the interband optical matrix element between the conduction and valence bands and γ_{N_c,N_v} is the broadening parameter of the Lorentzian function. The value $E_g = 1.51$ eV for GaAs has been used [9]. The theoretical formalism to calculate the dielectric constant in SAQLs was given in Ref. [26].

Figure 3 shows the dielectric constant for a SAQL of InAs embedded in a GaAs matrix for incident light propagating along the z-axis and polarized in the plane of the SAQL base. The SAQL in Fig. 3(a)

Table 1 Parameters used in the calculation of the dielectric constant.

parameters	InAs
E_g (eV)	0.45[a]
m_e^*/m_0	0.023[a]
m_{hh}^*/m_0	0.34[a]
m_{lh}^*/m_0	0.027[a]
ΔE_c (%)	40%[a]
ΔE_v (%)	60%[a]
P^2/m_0 (eV)	10.0[b]
γ_{hh} (meV)	3
γ_{lh} (meV)	5

[a] Ref. [9], [b] Ref. [33]

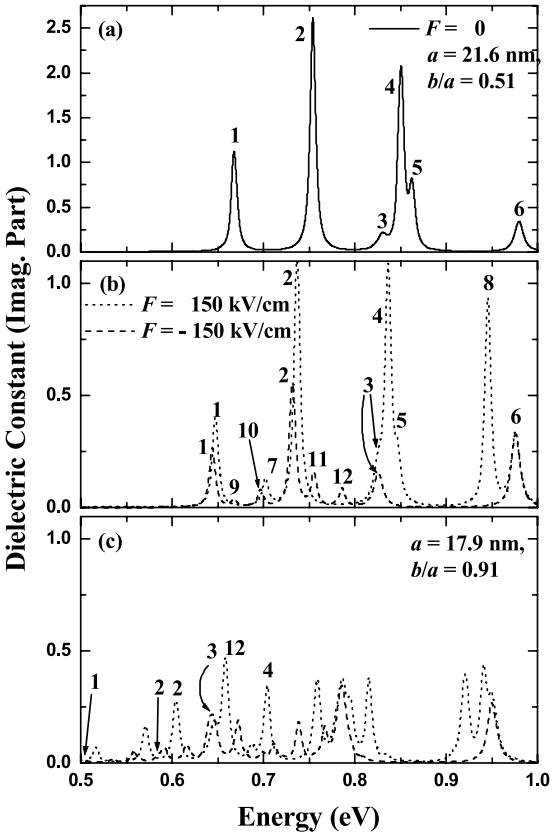

Fig. 3 Dielectric constant for InAs/GaAs SAQLs. (a) $a = 21.6$ nm and $b = 11.0$ nm. (b) Same configuration as in (a). (c) $a = 17.9$ nm and $b = 16.3$ nm. Both configurations have the same volume. Solid line represents the case with $F = 0$, while dotted (dashed) line the case $F = 150$ ($F = -150$) kV/cm.

and (b) has radius $a = 21.6$ nm and height $b = 11.0$ nm, while in Fig. 3(c) the configuration has the same volume but $a = 17.9$ nm and $b = 16.3$ nm. Three values of the electric field are considered: $F = 0$ (solid line) in Fig. 3(a) and $F = 150$ kV/cm (dotted line) and $F = -150$ kV/cm (dashed line) in (b) and (c). The complete range of the band offset is not shown, but only an energy relevant range where the first transi-

Table 2 Data corresponding to the transitions labelled in Fig. 3(a) and (b).

label	quantum numbers (N_c, N_v; m)	valence band	oscillator strength at F (kV/cm)		
			0	−150	150
1	(1,1;0)	hh	1.0	0.465	0.579
2	(1,1;1)	hh	1.0	0.450	0.640
3	(1,1;0)	lh	1.0	0.977	0.977
4	(1,1;2)	hh	1.0	–	0.697
5	(2,2;0)	hh	1.0	–	0.548
6	(1,1;1)	lh	1.0	0.981	0.982
7	(1,5;0)	hh	0.0	0.004	0.344
8	(1,1;3)	hh	0.0	–	0.745
9	(1,2;0)	hh	0.0	0.160	<0.05
10	(1,4;0)	hh	0.0	0.262	$<10^{-3}$
11	(1,2;1)	hh	0.0	0.24	<0.06
12	(1,4;1)	hh	0.0	0.182	$<10^{-2}$

tion takes place. In Table 2 the quantum numbers for the transitions in Fig. 3 are denoted by $(N_c, N_v; m)$, where N enumerates the electronic energies by increasing value for a fixed value of m. Moreover, the numbers $(N_c, N_v; m)$ indicate that the transition takes place from level N_v of the valence band (hh or lh) to level N_c at the conduction band. Also specified are the oscillator strengths at zero, -150 and 150 kV/cm. The symbol "–" means that the transition does not occur because the corresponding level in the conduction band is not present.

Comparing Fig. 3(a) and (b) it is clearly seen that for transitions 1 to 6 the peak energies are red-shifted at $F = \pm 150$ kV/cm with respect to their positions at $F = 0$ (Stark effect). Nevertheless, in Fig. 3(b) it can be seen that these displacements are not quantitatively the same for positive or negative field. For example, the transition peaks labelled by 1 and 2 do not appear at the same energy leading to $\delta(F) \neq 0$ for both cases.

On the other hand, the oscillator strengths for transitions at $F = 0$ are in general higher than their corresponding values for $F = \pm 150$ kV/cm due to the mixture of states caused as the electric field is turned on. Notice that in Fig. 3(a) the scale of the dielectric constant is twice the one used in Fig. 3(b) and (c). Furthermore, transition 6 originates in the light-hole valence band and comparing it in Fig. 3(a) and (b) we conclude that the transitions for the lh band are less affected by the electric field, due to the lower effective mass than in the case of the hh-valence band.

It can also be seen that the transitions from valence to conduction bands with $m \neq 0$ are relatively stronger than those with $m = 0$, for a given value of the electric field. Compare for example, transition 2 which has $m = 1$ (see Table 2) with transition 1 with $m = 0$. It is a consequence of the excitonic breaking of degeneracy. In the case of a transition with $(N_c, N_v, m = 0)$ the excitonic couple does not break the degeneracy. However, for a transition with $(N_c, N_v, m \neq 0)$, a three-fold level splitting is obtained. See details in Ref. [26]. The splitting levels remain very close each other causing closely spaced peaks which give rise to an enhanced dielectric signal.

Forbidden transitions at zero field are allowed at $F \neq 0$ and some of them are tuned at $F = \pm 150$ kV/cm in different ways, according to the direction of the applied field. See for example transitions 7, 9, 10, 11 and 12. In the case of transition 9, its oscillator strength at $F = 150$ kV/cm is so small that does not yield a visible peak, but this transition is noticeable for $F = -150$ kV/cm. On the other

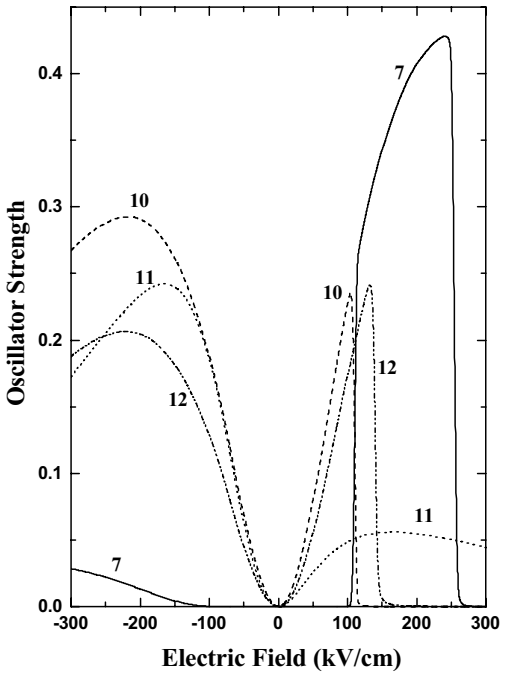

Fig. 4 Oscillator strength as function of the electric field for electron–hole transitions 7, 10, 11 and 12 which correspond to Fig. 3.

hand, transition 8 only appears at $F = 150$ kV/cm because the corresponding level does not exist at the conduction band for $F = -150$ kV/cm.

In Fig. 3(c) the domain has the same volume as in Fig. 3(a) and (b), but now the parameter $b/a = 0.91$. The transitions take place this time at lower energies, as seen in the figure. This shift is due to the softer confinement, for the lens has a shape almost semi-spherical. For the same reason, the effects of the electric field are reinforced, see Fig. 1. Thus, the mixing of the wavefunctions becomes stronger and, as a consequence, the oscillator strengths are more homogeneously distributed among all the possible transitions giving rise to rich peak distributions with quantum numbers $N_v \neq N_c$. For the same reason, the peak heights are smaller compared to those of Fig. 3(b). Differences in the energies for which transitions 1 and 2 occur are bigger than in Fig. 3(b), in agreement with the result obtained in Fig. 1.

For a better understanding of the peaks distribution in the dielectric constant, in Fig. 4 the oscillator strengths for transitions 7, 10, 11 and 12 are plotted as a function of the electric field. We can see a strong variation of the oscillator strength for transitions 7, 10 and 12 in a small range of positive values of the electric field. For transitions labelled with 7 and 10 this variation is a consequence of an anticrossing effect around $F = 100$ kV/cm, between the corresponding energy levels $N_v = 5$ (in transition 7) and $N_v = 4$ (in transition 10) for the hh-valence band with $m = 0$ (see Table 2). Similarly, transition 12 has a sharp variation at $F \approx 150$ kV/cm because of an anticrossing of the corresponding valence band at this value of the electric field. Then, it is possible to say that for some transitions the intensity of the dielectric signal vanishes at certain values of the electric field and a given lens configuration, leading to a non-monotonic behavior of the oscillator strengths as a function of the electric field.

3.1 Electroabsorption

The optical properties of the semiconductor structure have led to the most powerful techniques to study the electronic properties in solids [34]. Absorption [5, 8, 13, 35] and particularly electroabsorption [36] measurements are techniques used to inquire about the fundamental properties of different quantum structures. The relation between the imaginary part of the dielectric constant ε_2 and the absorption coefficient α is given by [34]

$$\varepsilon_2(\omega) = \frac{nc}{\omega}\,\alpha(\omega)\,, \tag{6}$$

where n is the real part of the refractive index and c the speed of light. We obtained the real part of the refractive index according to

$$n = \sqrt{\frac{\sqrt{\varepsilon_1^2 + \varepsilon_2^2} + \varepsilon_1}{2}} + n_\infty\,, \tag{7}$$

where ε_1 and ε_2 are the real and the imaginary part of the dielectric constant, respectively, and n_∞ is the high-frequency refractive index. For the case of an InAs SAQL we take $n_\infty = 3.517$ [33]. ε_1 is calculated from ε_2 and the Kramers–Kronig relations [26].

Previous studies [36, 37] have used the absorption change $\Delta\alpha(\omega, F) = \alpha(\omega, F) - \alpha(\omega, 0)$ of a SAQL as a tool to study low-dimensional structures. In our case, we study the absorption change for the two configurations used in Fig. 3. Different values of $\Delta\alpha$ will be obtained according to F being positive or negative. The results are shown in Fig. 5. In Fig. 5(a) the lens configuration of Fig. 3(a) and (b) has been used while in Fig. 5(b) the lens configuration corresponds to Fig. 3(c). In both cases, the dotted (dashed) line represents $\Delta\alpha$ for $F = 150$ ($F = -150$) kV/cm. Typical electroabsorption spectra are obtained and they depend on the direction of the electric field. A close correspondence is observed among the peak positions in this figure and the transitions shown in the dielectric constant (Fig. 3). Some transitions have been indicated for comparison. $\Delta\alpha$ depends on the direction of the electric field due to the spatial asymmetry of the lens, confirming that not only the magnitude but also the direction of the field is important.

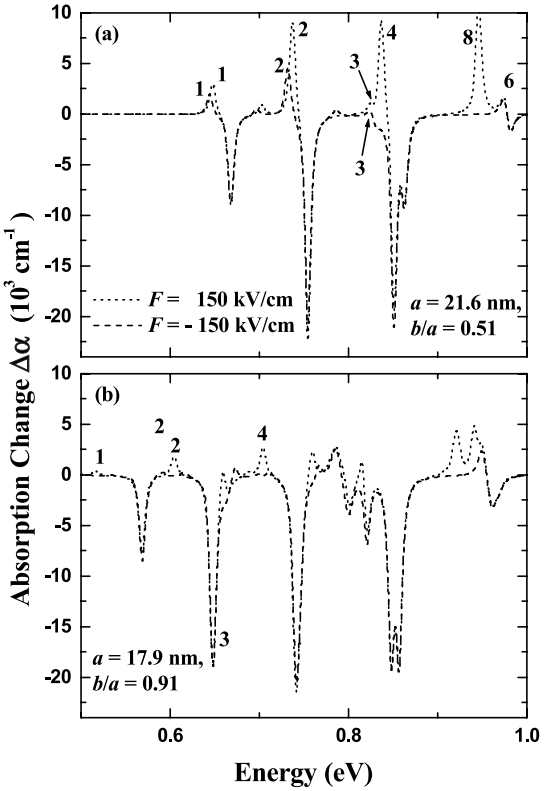

Fig. 5 Electroabsorption as a function of the energy. (a) Configuration corresponding to Figs. 3(a) and 3(b), and (b) configuration corresponding to Fig. 3(c).

Since this effect becomes important for stronger confinement, the peak heights turn out to be larger as Fig. 5(a) shows. Thus, electroabsorption measurements would provide signatures of the electronic structure of the SAQL.

4 Conclusions

The present work has studied the influence of the lens asymmetry along the axial axis on its electronic properties. The difference in the energy Stark-shift was characterized with the parameter $\delta(F)$, which measures the separation of the ground state transition energy as electric fields with same intensity have positive or negative direction along the axial symmetry axis. It was shown that the parameter $\delta(F)$ increases for high values of the field and diminishes as the lens deformation becomes larger (smaller ratio b/a). Nevertheless, even in this latter case the eigenvalues of the lens domain can not be approximated by those of a cylindrical domain with the same volume. Therefore, the full lens geometry must be always considered to obtain the correct spectrum.

The consequences of this asymmetry on the dielectric constant of the SAQL were also studied. We analyzed its behaviour as a function of the lens deformation for a fixed volume of the domain and a given absolute value of the field. Different transitions are obtained depending on the lens deformation b/a, the radius a and the magnitude and direction of the external field. We emphasize the importance of the direction of the electric field in the optical properties, such as the absorption change, showing different behaviour according to a positive or negative direction along the axis lens. Thus, in an experimental set up, an specific transition could be tuned. Moreover, the correlation between the electroabsorption peaks (shown in this work) and the electronic structure of the quantum lens (see details in Ref. [26] and references therein) can be useful in characterizing the geometrical dimensions of these semiconductor nanostructures.

Acknowledgments This work was partially supported by Grant II 193-04/EXG/G (VIEP-BUAP). We also thank C. Trallero-Giner for clever discussions.

References

[1] A. D. Yoffe, Adv. Phys. **50**, 1 (2001).
[2] L. Jacak, P. Hawrylak, and A. Wojs, Quantum Dots (Springer-Verlag, Berlin, 1998).
[3] I. N. Stranski and L. Krastanow, Sitz.ber. Akad. Wiss. Wien **146**, 797 (1938).
[4] M. A. Cusack, P. R. Briddon, and M. Jaros, Phys. Rev. B **54**, R2300 (1996).
[5] M. A. Cusack, P. R. Briddon, and M. Jaros, Phys. Rev. B **56**, 4047 (1997).
[6] M. Grundmann, O. Stier, and D. Bimberg, Phys. Rev. B **52**, 11969 (1995).
[7] C. Pryor, Phys. Rev. B **57**, 7190 (1998).
[8] O. Stier, M. Grundmann, and D. Bimberg, Phys. Rev. B **59**, 5688 (1999).
[9] E. Menéndez-Proupin, C. Trallero-Giner, and S. E. Ulloa, Phys. Rev. B **60**, 16747 (1999).
[10] E. C. Niculescu, phys. stat. sol. (b) **226**, 385 (2001).
[11] J. L. Marín, R. Riera, and S. A. Cruz, J. Phys.: Condens. Matter **10**, 1349 (1998).
[12] E. Menéndez, C. Trallero-Giner, and M. Cardona, phys. stat. sol. (b) **199**, 81 (1997).
[13] T. Uozumi et al., Phys. Rev. B **59**, 9826 (1999).
[14] A. Forchel et al., Semicond. Sci. Technol. **11**, 1529 (1996).
[15] X. Z. Liao et al., Phys. Rev. B **58**, R4235 (1998).
[16] J. H. Zhu, K. Brunner, and G. Abstreiter, Appl. Phys. Lett. **72**, 424 (1998).
[17] I. Hapke-Wurst et al., Semicond. Sci. Technol. **14**, L41 (1999).
[18] J. Zou, X. Z. Liao, D. J. H. Cockayne, and R. Leon, Phys. Rev. B **59**, 12279 (1999).
[19] P. W. Fry et al., Phys. Rev. Lett. **84**, 733 (2000).
[20] A. Wojs, P. Hawrylak, S. Fafard, and L. Jacak, Phys. Rev. B **54**, 5604 (1996).
[21] A. H. Rodríguez, C. R. Handy, and C. Trallero-Giner, J. Phys.: Condens. Matter **15**, 8465 (2003).
[22] E. Casado and C. Trallero-Giner, phys. stat. sol. (b) **196**, 335 (1996).
[23] I. Shtrichman et al., Phys. Rev. B **65**, 081303 (2002).
[24] A. H. Rodríguez and C. Trallero-Giner, phys. stat. sol. (b) **230**, 463 (2002).
[25] A. H. Rodríguez, L. Meza-Montes, C. Trallero-Giner, and S. E. Ulloa, phys. stat. sol. (b) **242**, 1820 (2005).
[26] A. H. Rodríguez, C. Trallero-Giner, M. Muñoz, and M. C. Tamargo, Phys. Rev. B **72**, 045304 (2005).
[27] Q. Xie, A. Madhukar, P. Chen, and N. P. Kobayashi, Phys. Rev. Lett. **75**, 2542 (1995).
[28] S. Li, J. Xia, Z. L. Yuan, and Z. Y. Xu, Phys. Rev. B **54**, 11575 (1996).
[29] S. Li and J. Xia, Phys. Rev. B **55**, 15434 (1997).
[30] S. Raymond et al., Phys. Rev. B **58**, R13415 (1998).
[31] A. H. Rodríguez and C. Trallero-Giner, J. Appl. Phys. **95**, 6192 (2004).
[32] M. Muñoz et al., Appl. Phys. Lett. **83**, 4399 (2003).
[33] Landolt Börnstein Tables, Vol. 37a of Landolt-Börnstein New Series, Group III, edited by O. Madelung (Springer-Verlag, Berlin, 1982).
[34] M. Dressel and G. Grüner, Electrodynamics of Solids: optical properties of electron in matter (University Press, Cambridge, 2002).
[35] N. Taniguchi and V. N. Prigodin, Phys. Rev. B **54**, 14305 (1996).
[36] K. Tanaka, T. Takahashi, and T. Kondo, Phys. Rev. B **71**, 045312 (2005).
[37] F. Henneberger, S. Schmitt-Rink, and E. O. Gödel (Eds.), Optics of Semiconductor Nanostructures (Akademie Verlag, Berlin, 1993).

